A microcalorimetric and microscopic strategy to assess the interaction between dietary fibers and small molecules

Author(s):
Lupo, Cristina; Boulos, Samy; Gramm, Fabian; Wu, Xiaowen; Nyström, Laura

Publication date:
2022-07-01

Permanent link:
https://doi.org/10.3929/ethz-b-000541621

Originally published in:
Carbohydrate Polymers 287, https://doi.org/10.1016/j.carbpol.2022.119229

Funding acknowledgement:
679037 - Soluble dietary fibre: unraveling how weak bonds have a strong impact on function (EC)

Carbohydrate Polymers 287 (2022) 119229

Contents lists available at ScienceDirect

Carbohydrate Polymers

journal homepage: www.elsevier.com/locate/carbpol

A microcalorimetric and microscopic strategy to assess the interaction between dietary fibers and small molecules

Cristina Lupo [a], Samy Boulos [a], Fabian Gramm [b], Xiaowen Wu [a], Laura Nyström [a,*]

[a] Department of Health Science and Technology, Institute of Food, Nutrition and Health, ETH Zurich, 8092 Zurich, Switzerland
[b] Scientific Center for Optical and Electron Microscopy, ETH Zurich, 8093 Zurich, Switzerland

ARTICLE INFO

Keywords:
Water-soluble dietary fibers
Small molecules
Thermodynamic parameters
Glyco-nanoparticles
Isothermal titration calorimetry
Transmission electron microscopy

ABSTRACT

The interaction between small molecules and neutral soluble dietary fiber is one of the proposed mechanisms determining the bioavailability of these components in the small intestine. However, the weak nature of these interactions makes it difficult to find an analytical method sensitive enough to detect them. Here, we probed the molecular interaction between galactomannan, arabinoxylan, and β-glucan with gallic acid, cinnamic acid, acetylsalicylic acid, and acetaminophen, using advanced analytical methods, namely isothermal titration calorimetry (ITC) and in the form of gold-nanoparticles, transmission electron microscopy (TEM). The results obtained from ITC analysis were fully consistent with the results obtained from TEM. In short, the interaction of these fibers and small molecules was mainly entropically driven, hence involving hydrophobic type association and possible conformational changes of the polysaccharide. However, the enthalpy contribution (hydrogen interaction) is also significant, especially regarding interactions with the acetylsalicylic acid molecule.

1. Introduction

Daily consumption of dietary fibers (DFs) is inarguably one of the most important habits that promote a healthy lifestyle. Indeed, there is convincing evidence that dietary fiber consumption decreases the risk of developing a multitude of chronic diseases, such as coronary heart disease, diabetes, obesity, and certain gastrointestinal diseases (Anderson et al., 2009). There is a general acceptance among researchers that the physiological effects of water-soluble dietary fibers are mainly driven by their physicochemical properties such as viscosity, bulking ability, and binding ability, as well as their fermentability (Gallaher & Schaubert, 1990; Nishinari et al., 2020; Queenan et al., 2007). Among these properties, viscosity is certainly the one most frequently considered factor for attributing to the beneficial activities exerted by water-soluble dietary fibers. In general, the ultimate effect of viscosity-associated mechanisms results in an overall reduction in the bioavailability of nutritionally relevant compounds such as bile acids, sugars and toxins (Gunness & Gidley, 2010). For instance, in a study performed by Zacherl et al. (2011), an *in vitro* simulated digestion dialysis model was developed for the evaluation of the bile acid-retention capacity of dietary fibers such as oat-fiber containing 44% total DF and 22% cereal mixed linkage β-glucan. The study showed a limited diffusion of bile acid molecules through the dialysis membrane and reported a linear-logarithmic correlation between viscosity and bile acid-retention. In the same study the authors intentionally decreased the viscosity of oat fiber by heat-treatment to investigate whether variation in viscosity could influence the retention behavior (Zacherl et al., 2011). Oat fibers reduced in viscosity almost halved their holding capacity, reinforcing the concept that fiber viscosity has a significant role in determining its retention capacity. In another study carried out by Marasca et al. (2020) the molecular interaction between a mixture of bile salts and β-glucan extracts from oat and barley, either in the native form or modified by partial hydrolysis or oxidation, was performed using equilibrium dialysis methodology. This study showed that bile acid retention was strongly dependent on fiber viscosity, whereby more viscous samples showed an enhanced effect in delaying the permeation of bile acids through the dialysis membrane.

Although there is experimental evidence associating the retention capacity of soluble dietary fibers to their viscosity, it is unlikely that the beneficial effect exerted by these macromolecules is purely and exclusively the result of their rheological properties. For example, it was reported by Edwards et al. (1987) that decrease in glucose response was not solely influenced by the effect of viscosity on gastric emptying. The

* Corresponding author.
E-mail addresses: cristina.lupo@hest.ethz.ch (C. Lupo), samy.boulos@hest.ethz.ch (S. Boulos), fabian.gramm@scopem.ethz.ch (F. Gramm), xiaowen.wu@hest.ethz.ch (X. Wu), laura.nystroem@hest.ethz.ch (L. Nyström).

https://doi.org/10.1016/j.carbpol.2022.119229
Received 12 October 2021; Received in revised form 3 February 2022; Accepted 4 February 2022
Available online 8 February 2022

gastric emptying function was monitored in volunteers upon ingestion of glucose-enriched guar gum, locust bean, and xanthan gum, or a combination of these last two fiber solutions. The authors concluded that reduction in gastric emptying, and thus the viscosity of the fibers may not be the only mechanism of altered glycemic response *in vivo*. This observation leads to the hypothesis that the beneficial effect exerted by dietary fibers (retaining nutrients and other compounds from absorption) is not solely related to their viscosity but also to the specific structure of the polysaccharide, whereby precise binding interactions on a molecular level between fiber and target molecules may contribute equally. However, the precise mechanism underlying these molecular interactions still remains to be clarified. Until today, the *in vitro* methods and analytical approaches proposed in literature to verify this new hypothesis have usually assessed the interactions between ionic polysaccharides with neutral or charged ligand molecules. In these studies the relatively strong ionic interaction is easy to detect and measure. For example, the interaction between anthocyanins and pectin was evaluated by UV–vis and saturation transfer difference (STD) NMR spectroscopy (Fernandes et al., 2014). The results showed that hydrogen bonds established between the hydroxyl groups of the anthocyanins and the pectin's galacturonic acid moieties, as well as hydrophobic contact between pectin residues and the planar surfaces of anthocyanins, were the main molecular mechanisms underlying of interaction. Similarly, ionic interactions could be measured between anionic polyelectrolyte carrageenans and a cationic amphiphilic drug using an ion-selective membrane electrode (Pavli et al., 2011). The most important outcome derived from this analysis was the discovery of cooperative mechanism between an initial electrostatic factor between the drug and the polysaccharides, followed by supramolecular self-assembly interaction between different drug molecules in the vicinity of the polysaccharide, leading to the formation of charged aggregates which interact with sulphate ester groups of the anionic polysaccharide.

In contrast to the interactions between charged fibers and ligands, research concerning the binding between neutral, uncharged soluble polysaccharides and small molecules are scarce in literature. To better understand such interactions and their relevance in nutrition, as well as to maximize beneficial effects associated with neutral fiber consumption, it is necessary to understand the binding mechanism governing these low-affinity associations. Phenolic compounds and drugs are examples of molecules that have important beneficial and therapeutic effects on humans. On one hand, phenolic compounds have demonstrated positive effects on human health. They can inhibit the proliferation of tumors cells, reduce vascularization, protect neurons from oxidative stress, stimulate vasodilation and improve insulin secretion (Kahkeshani et al., 2019). On the other hand, the interaction between dietary fiber and orally administered drugs could lower their therapeutic effect, if the absorbability drug is reduced due to the interaction with the fiber. Hence, to be able to ensure the efficacy of the drugs, it is of importance to be able to assess such weak interactions. Therefore, in this study, we propose a unique approach for the synthesis of neutral-soluble dietary fiber-tethered gold nanoparticles to elucidate the possible key parameters underlying the association between neutral soluble polysaccharides with small molecules, namely galactomannan (GM), arabinoxylan (AX), and mixed linkage cereal β-glucan (BG) with different nutritionally relevant small molecules and drugs: gallic acid (GA), trans-cinnamic acid (*t*-CA), acetylsalicylic acid (ASA), and acetaminophen (ACM). Specifically, isothermal titration calorimetry (ITC) was employed to screen the interaction between the small molecules and GM, AX, and BG, allowing to determine whether a direct interaction with a target molecule occurs, and to calculate essential parameters of the biomolecule-ligand interaction, such as the binding dissociation constant (K_d), the binding stoichiometry (N), the binding enthalpy (ΔH) and binding entropy (ΔS), while also providing information on the nature of the non-covalent forces responsible for the interaction. Moreover, thiolated fibers were used for the self-assembly reaction onto the surface of gold nanoparticles, and potential interaction was revealed using transmission electron microscopy TEM by monitoring the spatial arrangement of the glyco-nanoparticles (glyco-AuNPs) before and after the addition of the small molecule. Until today, glyco-nanoparticle (glyco-NP) functionalization has only been reported with monosaccharides or short oligosaccharides, which is not suitable for the study of the fiber polysaccharide interactions that requires the longer polysaccharide chains. Therefore, our strategy using glyco-NPs with tethered polysaccharide chains is therefore novel for the interaction studies.

Given the few studies reported in literature on interaction between neutral polysaccharides and small molecules, this research demonstrates that the combination of nanotechnology with advanced microcalorimetry and microscopy techniques is a valid alternative to study the interaction of two molecules, giving a better understanding of the molecular mechanisms that underlie these weak associations and thus providing information on structure-function-property relationship. In addition, this work used chemically functionalized nanoparticles with structurally different high molecular weight polysaccharides as a flexible and sensitive method for TEM interaction studies.

2. Materials and methods

2.1. Materials

Tetrachloroauric acid trihydrate ($HAuCl_4 \cdot 3H_2O \geq 99.0\%$), distilled water (DI), nitric acid (HNO_3 70.0%), concentrated hydrochloric acid (HCl, 37%), tri-sodium citrate dihydrate ($Na_3C_6H_5O_7 \cdot 2H_2O \geq 99.0\%$), sodium phosphate dibasic (Na_2HPO_4, 99.95%), isopropanol (i-PrOH, ≥99.7%), sulfuric acid (H_2SO_4, ACS reagent, 95.0–98.0%), anthrone (ACS reagent, 97.0%), borane dimethylamine complex (DMAB, ≥97.0%), sodium (meta)periodate ($NaIO_4$, ≥99.0%), ethylene glycol ($(CH_2OH)_2$, ReagentPlus®, ≥99.0%), 4-aminophenyl disulfide (APDS, ≥99.0%), acetic acid (CH_3COOH, glacial, ReagentPlus ®, ≥99%), gallic acid (GA, ≥98.0%), trans-Cinnamic acid (t-CA, ≥99.7%), acetylsalicylic acid (ASA, ≥99.0%) and acetaminophen (ACM, analytical standard) were purchased from Sigma-Aldrich (St. Louis, MI, USA). Deuterium oxide (D_2O, 99.9%) was purchased from Cambridge Isotope Laboratories, Inc. (Andover, MA, USA). Guar galactomannan (GM) high viscosity (Gal depleted, viscosity >10 dL/g, $M_w = 350$ kDa, sugar ratio Gal:Man = 21:79 (Lot#10502 B)), wheat arabinoxylan (AX) medium viscosity (viscosity 20–30 cSt, $M_w = 323$ kDa, sugar ratio Ara:Xyl = 38:62 (Lot#40601 A)) and oat β-glucan (BG) standard (intrinsic viscosity 1.32 dL/g, $M_w = 70.6$ kDa (Lot#110303 A)) was purchased from Megazyme (Bray, Ireland). The monosaccharide ratio of GM and AX provided in the product specifications by Megazyme were slightly different than those obtained through analysis by high-performance anion-exchange chromatography-pulsed amperometric detection (HPAEC-PAD) after complete acid hydrolysis of the polysaccharides (Guar galactomannan (GM), sugar ratio Gal:Man = 17:83 (Lot#10502 B)), wheat arabinoxylan (AX), sugar ratio Ara:Xyl = 35:65 (Lot#40601 A)). All aqueous solutions were prepared using Milli-Q water (Milli-Q® IQ 7000 Ultrapure Water System, Merck Millipore, Darmstadt, Germany). Dialysis membranes made from regenerated cellulose with MWCO 12,000–14,000 Da (25 Å; 29 mm) were supplied by SERVA (Heidelberg, Germany). All reagents were used as received without further purification.

2.2. Synthesis and characterization of thiol-derivatized dietary fibers

2.2.1. Partial acid hydrolysis, controlled oxidation, and conjugation with thiol linker of GM, AX and, BG

Low dispersity ($Đ$) and molecular weight (M_w) galactomannan and arabinoxylan were produced by a partial acid hydrolysis for 24 h and 3 h, respectively, followed by *i*-PrOH precipitation, as described previously (Lupo et al., 2020). For more details on the partial acid hydrolysis protocol see supplementary information. Standard oat β-glucan was used as received without further purification. Partially hydrolyzed

polysaccharides (GM_{HCl} and AX_{HCl}) obtained from the acid treatment, and standard β-glucan (BG) were reacted with $NaIO_4$, followed by a reductive amination reaction, as described previously (Lupo et al., 2021). The selection of the GM_{HCl} and AX_{HCl} fractions used in the oxidation and functionalization steps with the thiol linker was based on the lower dispersity, better purity and higher gravimetric yield of the fiber samples obtained after isopropanol fractionation of the hydrolyzed polysaccharides (see Table S2 in the supplementary materials). Moreover, the lower viscosity of these fractions allowed a better filling of the ITC sample cell and therefore a better performance of the calorimetric polysaccharide-ligand interaction experiment. Briefly, 14.29 μM, 10.77 μM BG, and 0.94 μM of GM_{HCl}, BG, and AX_{HCl} solutions, respectively, were prepared in water under agitation for 24 h, respectively. After complete dissolution, all the polysaccharide solutions were treated with 2 equiv. (with respect to the polysaccharide chains according to their M_n) of an aqueous 47 mM $NaIO_4$ solution and reacted for 6 h in the dark at room temperature. Then, 2 equiv. ethylene glycol were added to quench the reaction. Afterwards, the oxidized products were purified by dialysis against water for 12 h, precipitated with two volumes of *i*-PrOH and freeze-dried for 48 h. Solid oxidized sample solutions (GM_{OX}(0.36 mM), AX_{OX} (0.12 mM) and BG_{OX} (0.29 mM)) were then reacted with 50 mM 4-aminophenyldisulfide (APDS) solution, previously prepared in water:acetic acid = 1:1. The polysaccharide and thiol-linker solutions were stirred for 1 h at 30 °C. Thereafter, the appropriate amount of solid dimethylamine borane was added to each of the mixtures at 100 mM final concentration, and the reactions were stirred unsealed for 1 h at room temperature. Then, the solutions were resealed and incubated for 1 h at 50 °C. All the thiolated fibers (GM_{SH}, AX_{SH} and BG_{SH}) were purified by dialysis for 48 h, freeze-dried for two nights and stored at −20 °C in the dark. For the chemical structure of the native and modified fiber samples see supplementary information (Fig. S1).

2.2.2. Molecular weight (M_w and M_n) and dispersity (Đ) analysis

Hydrolyzed, oxidized and thiolated fibers were analyzed for their molecular weight and dispersity by high-performance size exclusion chromatography (HPSEC) (OMNISEC, Malvern Panalytical Ltd., Malvern, UK) following the procedure previously published (Lupo et al., 2020). Briefly, the mobile phase consisted of a 0.1 M $NaNO_3$ with 0.02% NaN_3 solution. Samples were dissolved in the mobile phase at a concentration of 0.1% (w/v) and filtered through a 0.45 μm nylon filter prior to injection. The system was kept at 30 °C, and 100 μL of each sample were sequentially injected at a flow rate of 0.7 mL/min. For the absolute molecular weight determination, a calibration was performed using narrow molecular weight distribution polyethylene oxide (PEO-24 K) standard using the refractive index increment (dn/dc) value of 0.144 mL/g for galactomannan, 0.132 mL/g for arabinoxylan, and 0.145 mL/g for oat β-glucan. All samples were measured in triplicate. OMNISEC software version v.10.30 was used for data acquisition, analysis, and reporting.

2.2.3. Monosaccharide composition of hydrolyzed GM and AX by HPAEC-PAD

The monosaccharide ratio before and after acid treatment was measured by high-performance anion-exchange chromatography-pulsed amperometric detection (HPAEC-PAD) (Thermo Scientific AG, Basel, Switzerland). A complete hydrolysis of 50 mg of dried GM_{HCl} and AX_{HCl} was performed in 10 mL 2 M HCl solution at 100 °C for 45 min. After cooling to room temperature, the polysaccharide solutions were neutralized with 5 mL 4 M NaOH and centrifuged for 15 min at 4000 rpm. The hydrolysates were diluted with water to reach a concentration of 10 mg/L and filtered through a 0.45 μm PTFE filter.

A ICS-5000 system was used for the analysis, and an isocratic method was applied based on the procedure described previously (Eder et al., 2021). Briefly, the column was operated at 26 °C using a flow rate of 1.0 mL/min and injection volumes of 10 μL. The mobile phase consisted of two eluents: (A) 200 mM NaOH and (B) water. Specifically, 8% (A) and 92% (B) was run for the first 22.5 min, followed by 100% (A) for 8.5 min, and 8% (A) and 92% (B) for 8 min. For the external calibration, the concentration of the appropriate monosaccharide standards was within the range of 0.3–30.0 mg/L. D-Sorbitol was used as internal standard and added at a constant concentration of 10 mg/L to each sample and calibrant solution. The monosaccharides concentration was quantified relative to the internal standard signal. Data processing was carried out on Chromeleon 7 (Thermo Fischer Scientific AG, Basel, Switzerland). All samples were measured in triplicate.

2.2.4. Proton nuclear magnetic resonance (^1H NMR)

Thiolated polysaccharides were characterized using proton nuclear magnetic resonance (^1H NMR) to obtain the number of 4-aminothiolphenol linkers (ATP) per polymer chain. About 20 mg of GM_{SH}, AX_{SH}, and BG_{SH} were dissolved overnight in 1.2 mL D_2O. An aliquot of 700 μL of each solution was transferred into NMR tubes and analyzed by a Bruker AVANCE III-400 spectrometer (Bruker, Ettlingen, Germany) operating at room temperature at 400 MHz with 960 repetitive scans and an acquisition time of 4 s. Data processing was carried out on MestReNova 14 (Mestrelab Research SL, Santiago de Compostela, Spain). For all the polysaccharide samples the relative peak area of the anomeric proton signals were determined by setting the area of the aromatic ring protons (~7.4 and 6.8 ppm) equal to 2 and using the signal of residual water in D_2O at 4.79 ppm as an internal chemical shift reference. To determine the number of ATP molecules per polymer chain (n°(ATP)), slightly different calculation and spectra-processing procedure were used for the different fibers. For more details on the calculation procedure see supplementary information.

2.3. Synthesis and characterization of glyco-gold nanoparticles (glyco-AuNPs)

2.3.1. Synthesis of glyco-AuNPs from citrate-AuNPs and their characterization

Glyco-gold nanoparticles (GM_{SH}-AuNPs, AX_{SH}-AuNPs and BG_{SH}-AuNPs) were prepared based on the procedure described previously (Lupo et al., 2021). Firstly, citrate-capped gold nanoparticle (citrate-AuNPs) were synthesized following the Turkevich method (Balasubramanian et al., 2010). Briefly, 43 mg of $HAuCl_4 \cdot H_2O$ were dissolved in 100 mL water. The solution was heated to 100 °C under stirring (800 rpm). At the boiling point, 10 mL of a freshly prepared sodium citrate (38.8 mM) solution was quickly added (1.0 mM $HAuCl_4 \cdot H_2O$ final concentration). The mixture was heated for 15 min at 90 °C under stirring (800 rpm) within which a color change of the solution from colorless to purple occurred. The particle solution was stirred for an additional 20 min at 90 °C, afterward it was cooled to room temperature, and transferred into an amber bottle.

All the glyco-nanoparticle materials (glyco-AuNPs) were synthesized by adding into 18.8 mL of citrate-AuNPs solution 10.8 mg of the thiol-derivatized dietary fiber sample, previously synthesized as describe in Section 2.2.1. The mixtures were stirred for 48 h at room temperature in the dark. Excess thiolated polysaccharides were removed from the solution by washing the glyconanoparticle samples with water. Briefly, the glyco-nanoparticles were centrifuged at 23,710 ×*g* for 25 min, after which the supernatant solution was discarded and replaced with 10 mL water. After being resuspended, the glyco-AuNPs solution was centrifuged again, and the procedure described above was repeated two more times. Modified nanoparticles were resuspended in 17 mL water to give a concentration of about 8 nM Au particles.

2.3.2. UV–vis absorption, DLS and zeta potential measurements

Citrate-AuNPs and glyco-AuNPs solutions were characterized spectroscopically using a Cary 100 spectrophotometer (Agilent Technologies Inc., Santa Clara, CA, USA). A total of 500 μL citrate-AuNPs or glyco-AuNPs were diluted with 500 μL water, mixed, and placed in a 1 cm path length disposable polystyrene cuvette. The wavelength was

scanned from 350 nm to 700 nm and water was used as a blank. All the measurements were performed in triplicate.

In addition, the hydrodynamic diameter (d_h) and polydispersity index (PdI) of citrate-AuNPs and glyco-AuNPs were measured by dynamic light scattering (DLS) using the Zetasizer Nano-ZS (Malvern Instrument Ltd., Malvern, UK) while the net surface charge of the nanoparticle was determined by measuring the zeta potential (ζ) on the same instrument. Before analysis, 1 mL of sample solution was filtered through a 0.45 μm PTFE filter. All measurements were performed in triplicate.

2.3.3. Morphology and size distribution

A transmission electron microscope (FEI TalosTM F200X) operating at 200 kV was used to study the morphology and size distribution of the citrate- and glyco-AuNPs samples. Scanning transmission electron microscope acquisition (STEM) was used to analyses the sample in dark-field mode (HAADF). An aliquot of about 5 μL of the sample was dropped onto copper grids coated with carbon film (300 mesh). The excess solution was removed by absorption on absorbent paper after about 1 min. The STEM images were analyzed using ImageJ software. A total of about 300 particles were counted, and their area was measured. The average diameter (d) of the analyzed particle samples were calculated by the following equation

$$A\ (\mathrm{nm}^2) = \pi \bullet \mathrm{r}^2 \quad (1)$$

where A is the area of a circle and r is the radius. Knowing r of the particle, the diameter (d) was calculated as

$$d\ (\mathrm{nm}) = r \bullet 2. \quad (2)$$

2.3.4. Ligand surface density

The ligand surface density was evaluated using the anthrone/H_2SO_4 assay (Wang et al., 2009). Calibration curves were created using different concentrations of monosaccharide mixtures equivalent to the Gal:Man and Ara:Xyl molar ratio of the respective galactomannan and arabinoxylan samples, while glucose was used for β-glucan. The calibration for GM, AX and BG were in the range of 12–192 μg/mL, 6–96 μg/mL, and 1.5–24 μg/mL, respectively. Briefly, a total of 0.5 mL of each standard solution was transferred inside an amber bottle and stored in iced water under stirring. One mL of the freshly prepared anthrone solution (100 mg of anthrone into 50 mL of concentrated H_2SO_4) was added into the standard solutions. The samples were heated to 100 °C for 10 min under stirring. After that, the standard solutions were cooled in an iced water bath and the absorbance was measured at λ = 625 nm. The blank sample consisted of 1 mL of anthrone solution in 0.5 mL water, and the instrument was zeroed with water. All standards were measured in triplicate.

Glyco-AuNP solutions were extensively mixed and three aliquots of 0.5 mL each were placed inside an amber bottle previously cooled in an ice bath. The sample solutions were treated with anthrone reagent following the same procedure described for the standard solutions, with the exception that glyconanoparticles were reacted with the anthrone reagent for 20 min (Turula Jr et al., 2010). The blank sample consisted of 1 mL of anthrone solution in 0.5 mL water, and the instrument was zeroed with water. A control experiment was performed by measuring the absorbance of Glyco-AuNPs at λ = 625 nm in the absence of the anthrone reagent. All samples were measured in triplicate.

2.4. Interaction study

2.4.1. Interaction study with ITC

An isothermal titration calorimetry (MICROCAL PEAQ-ITC, Malvern Panalytical Ltd., Malvern, UK) was employed to measure the heat change that occurs when partially hydrolyzed GM_{HCl} and AX_{HCl} and standard β-Glucan (BG) were titrated with gallic acid (GA), trans-cinnamic acid (t-CA), acetylsalicylic acid (ASA), and acetaminophen (ACM). Briefly, the sample cell was loaded with 280 μL of 125 μM GM_{HCl}, 125 μM BG, or 62.5 μM of AX_{HCl} solution, previously prepared by dissolution in water overnight. The titration syringe was filled with aqueous solutions of the ligands at a concentration in the range of 0.625–1.25 mM, depending on the ligand and the polysaccharide (for exact concentrations, see Table S1). A total volume of 40 μL of the ligand was injected (2 μL/injection; 20 injections) in the sample cell containing the fiber. Each injection lasted 4 s, and an interval of 150 s was kept between injections. The experiments were conducted at 25 °C, and the fiber solutions were constantly stirred at 750 rpm throughout the titration experiment. Control experiments were performed under the same experimental conditions as described above and consisting of injection of ligands into the sample cell filled with water. Data analysis and reporting were performed with MicroCal PEAQ-ITC Analysis software using "one set of sites" fitting model to fit the measured binding isotherms and calculate the binding stoichiometry (N), the dissociation constant (K_d), enthalpy (ΔH), and entropy (ΔS) of the interaction.

2.4.2. Interaction study with TEM

Transmission electron microscopy (Thermo Fisher Talos F200X and Hitachi HD-2700) operating at 200 kV was used to visualize the interaction study between glyco-nanoparticles (GM_{SH}-AuNPs, AX_{SH}-AuNPs, and BG_{SH}-AuNPs) and the different small molecules, namely gallic acid (GA), *trans*-cinnamic acid (*t*-CA), acetylsalicylic acid (ASA) and acetaminophen (ACM). Scanning transmission electron microscope (STEM) acquisition was used to map the sample in a high angle annular dark field (HAADF) mode. For the experiment, 500 μL of glyco-AuNPs (8.0 nM) were incubated with 12.5 μL of 2 mM ligand solutions in water to have a final concentration of 50 μM ligand in each particle solution. The solutions were incubated under shaking for 3 h at room temperature. Afterward, 5 μL of each sample solution was placed onto a 300 mesh copper grid and the excess liquid was absorbed by paper tissue. The blank sample consisted of a 500 μL glyconanoparticle solution with 12.5 μL of water. Control experiments were conducted by subjecting the citrate-AuNPs to the same conditions as described above.

3. Results and discussion

3.1. Molecular weight (M_w and M_n), dispersity (Đ), and monosaccharide composition analysis

The dispersity and molecular weight of GM and AX after reaction with hydrochloric acid and subsequent fractionation with *i*-PrOH were evaluated by HPSEC to determine which of the collected polysaccharide fractions was most appropriate for the subsequent oxidation and reductive amination reaction. The second fraction of both fibers was the most suitable material for our purpose, as it was obtained with a moderate dispersity, and with a relatively satisfactory yield. More detailed characterization of the fractionated material can be found in the supplementary information (Table S2).

As expected, the acid-treated fibers resulted in a significantly lower molecular weight (M_w, M_n) in comparison to the untreated samples, while the molecular weight of standard β-Glucan provided in the product specifications by Megazyme was confirmed (Table 1). The 6-fold *vs.* 3-fold decrease in M_w to obtain GM_{HCl} and AX_{HCl}, respectively was mainly linked to the longer reaction hydrolysis time for galactomannan (24 h) than that for arabinoxylan (3 h), as described in the supplementary materials. For all the oxidized samples, a substantial reduction of their molecular weights was observed, in agreement with our previous publication and in line with other studies (Börjesson et al., 2018; Lupo et al., 2021; Marasca et al., 2020). Indeed, while periodate ion $[IO_4]^-$ cleaves the carbon-carbon bond of vicinal diols, several competitive reactions might occur, such as β-elimination, an over-oxidation of the reducing end of the polysaccharide, and a hydroxyl radical-mediated chain scission of glycosidic linkages induced by a

Table 1
M_w, M_n and $Đ$ measurements of GM, AX, and BG after 24 h acid hydrolysis followed by *i*-PrOH precipitation, after oxidation with $NaIO_4$, and after reductive amination with a thiol linker.

		M_w (kDa)	M_n (kDa)	$Đ$ (M_w/M_n)
Galactomannan (GM)				
Native GM	GM	313 ± 1	170 ± 2	1.80 ± 0.02
Acid-treated GM	GM_{HCl}	49 ± 1	33 ± 1	1.50 ± 0.02
Oxidized GM	GM_{OX}	28 ± 1	19 ± 1	1.50 ± 0.01
Thiolated GM	GM_{SH}	69 ± 9	60 ± 5	1.1 ± 0.1
Arabinoxylan (AX)				
Native AX	AX	321 ± 3	157 ± 1	2.0 ± 0.1
Acid-treated AX	AX_{HCl}	106 ± 2	76 ± 5	1.60 ± 0.01
Oxidized AX	AX_{OX}	86 ± 6	60 ± 2	1.50 ± 0.06
Thiolated AX	AX_{SH}	147 ± 2	104 ± 2	1.40 ± 0.01
β-Glucan (BG)				
Native BG	BG	65 ± 1	49.0 ± 0.3	1.30 ± 0.01
Oxidized BG	BG_{OX}	34 ± 1	24 ± 1	1.40 ± 0.02
Thiolated BG	BG_{SH}	65 ± 3	56 ± 1	1.2 ± 0.1

spontaneous decomposition of periodate in solution, leading to a reduction of the average degree of polymerization (Vold & Christensen, 2005).

The reductive amination of the oxidized polysaccharides with 4-aminophenyl disulfide (APDS) led to the formation of thiolated fibers with almost twice the molecular weight than that of the corresponding oxidized compounds, in agreement with a dimerization reaction in air, as well as in aqueous solution of the thiol group to disulfides (Bagiyan et al., 2003).

Monosaccharide composition and purity of acid-treated galactomannan and arabinoxylan was determined by HPAEC after complete hydrolysis of the samples. The galactose (Gal) to mannose (Man) ratio was determined to be 17:83 for the untreated galactomannan (GM) with 83% of purity, and 18:82 for acid-treated galactomannan (GM_{HCl}) with 73% of purity, whereas the arabinose (Ara) to xylose (Xyl) ratio of the untreated arabinoxylan sample (AX) was 35:65 with 79% of purity, while for the acid-treated arabinoxylan (AX_{HCl}), it was 27:73 with 69% of purity. The reduced purity found in hydrolyzed samples is probably moisture and not actual impurities, however it has always been taken into account for the calculation of the concentrations. For more information regarding the monosaccharide composition and purity of all fractions collected during the precipitation process with *i*-PrOH, refer to Table S2 in the supplementary section.

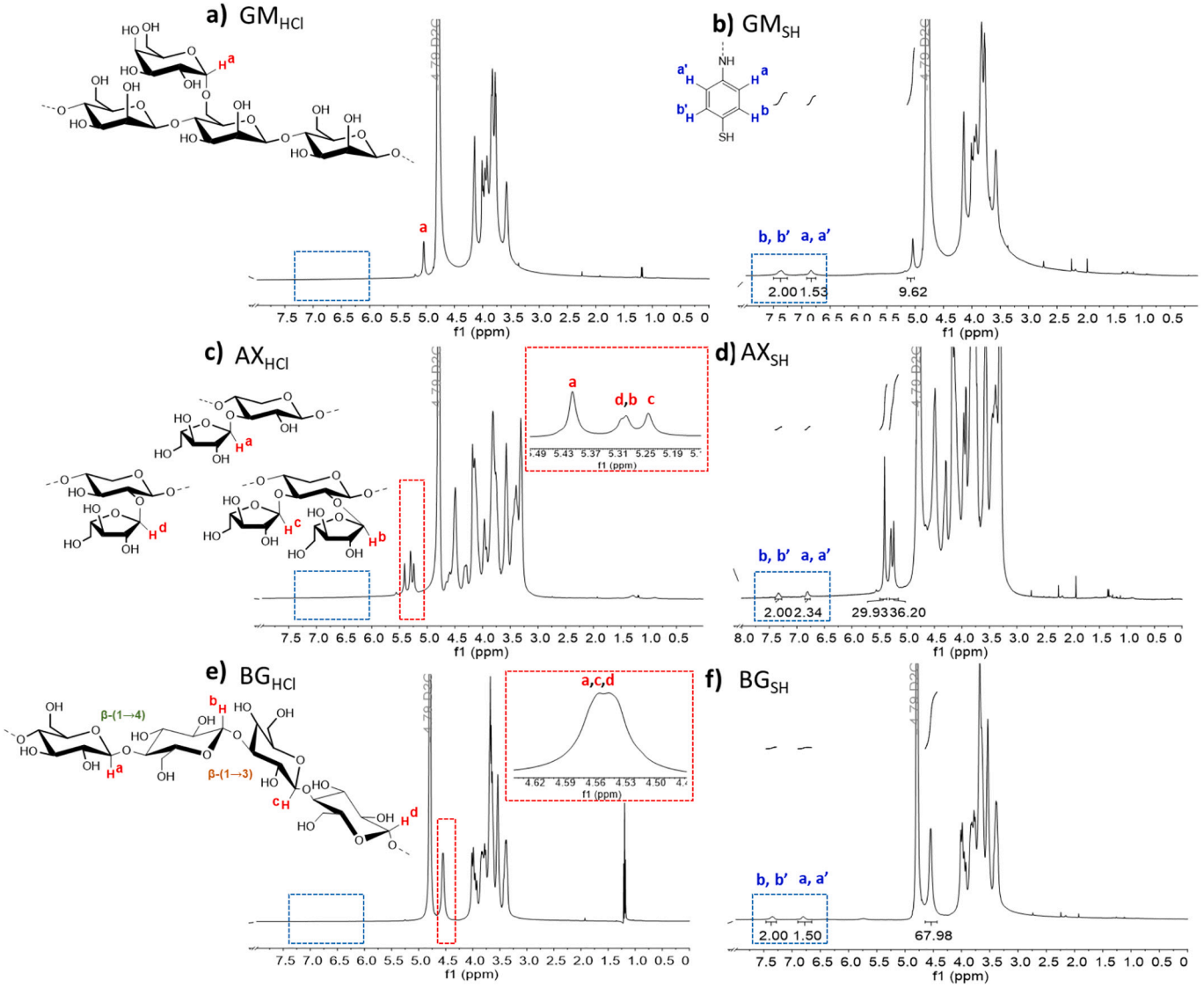

Fig. 1. ^1H NMR spectra in D_2O before thiol-derivatization a) GM_{HCl}, c) AX_{HCl}, e) BG, and after thiol-derivatization b) GM_{SH}; d) AX_{SH}; f) BG_{SH}.

3.2. Quantification of ATP coupling efficiency of thiolated dietary fibers via ^1H NMR

An inspection of the thiolated sample ^1H NMR spectra revealed the presence of typical signals corresponding to the two protons belonging to the aromatic ATP ring (~7.4 and 6.8 ppm), confirming the presence of the thiol linker on the galactomannan, arabinoxylan and β-glucan structure (Fig. 1b, d, f).

The signal H-1 of α-D-galactopyranose ring of galactomannan sample was found at ~5.03 ppm, while the typical peak related to the H-1 of β-D-mannopyranose ring that is usually at 4.75 ppm was overlapped with the solvent signal. The arabinoxylan spectra showed three peaks between 5.0 and 5.6 ppm which belong to the anomeric protons of α-L-arabinofuranosyl residues. Specifically, the peak at 5.40 ppm refers to the anomeric protons of the arabinose linked to the *O*-3 position of xylose residues, while the two peaks at 5.30 ppm and 5.24 ppm are from anomeric protons of arabinose residues linked to *O*-2 and *O*-3 of the same xylose residue. In addition, the anomeric proton of α-L-arabinofuranosyl residues linked to *O*-2 of the monosubstituted xylopyranosyl unit was observed at 5.30 ppm. Thiolated β-glucan sample showed a group of overlapped signals (a,c,d) at 4.55 ppm corresponded to protons of the (1 → 4)-linked β-D-glucopyranosyl units, while the proton (b) of 1,3-linked-β-D-glucopyranosyl unit is hidden under the solvent peak (Colleoni-Sirghie et al., 2003; Pitkanen et al., 2009; Tamaki et al., 2010). The number of 4-aminothiophenol tags (n°(ATP)) per polysaccharide chain was determined by ^1H NMR analysis following the calculation procedure describe in Section 2.2.4, with n°(ATP)-GM_{SH} = 4.5, n°(ATP)-AX_{SH} = 2 and n°(ATP)-BG_{SH} = 5.1. From the number of ATP tags per polymer chain, the percentage of modified monomeric units per polysaccharide chain was calculated. Specifically, a maximum modification of 1.2%, 0.3% and 1.5% was obtained for GM_{SH}, AX_{SH} and BG_{SH}, respectively. This means that in all derivatized samples ~98–99% of the monosaccharide units remain unchanged, making it more likely that the fiber properties should not be much affected, and that the modification does not influence the interactions too much. Especially considering that the label will mostly be right on the surface of the gold when in a glyco-AuNP, thus not very accessible compared to the rest of the chain, which can still interact with small molecules unimpededly.

3.3. Characterization of citrate- and glyco-gold nanoparticles

Variation on the gold surface plasmon resonance absorption band

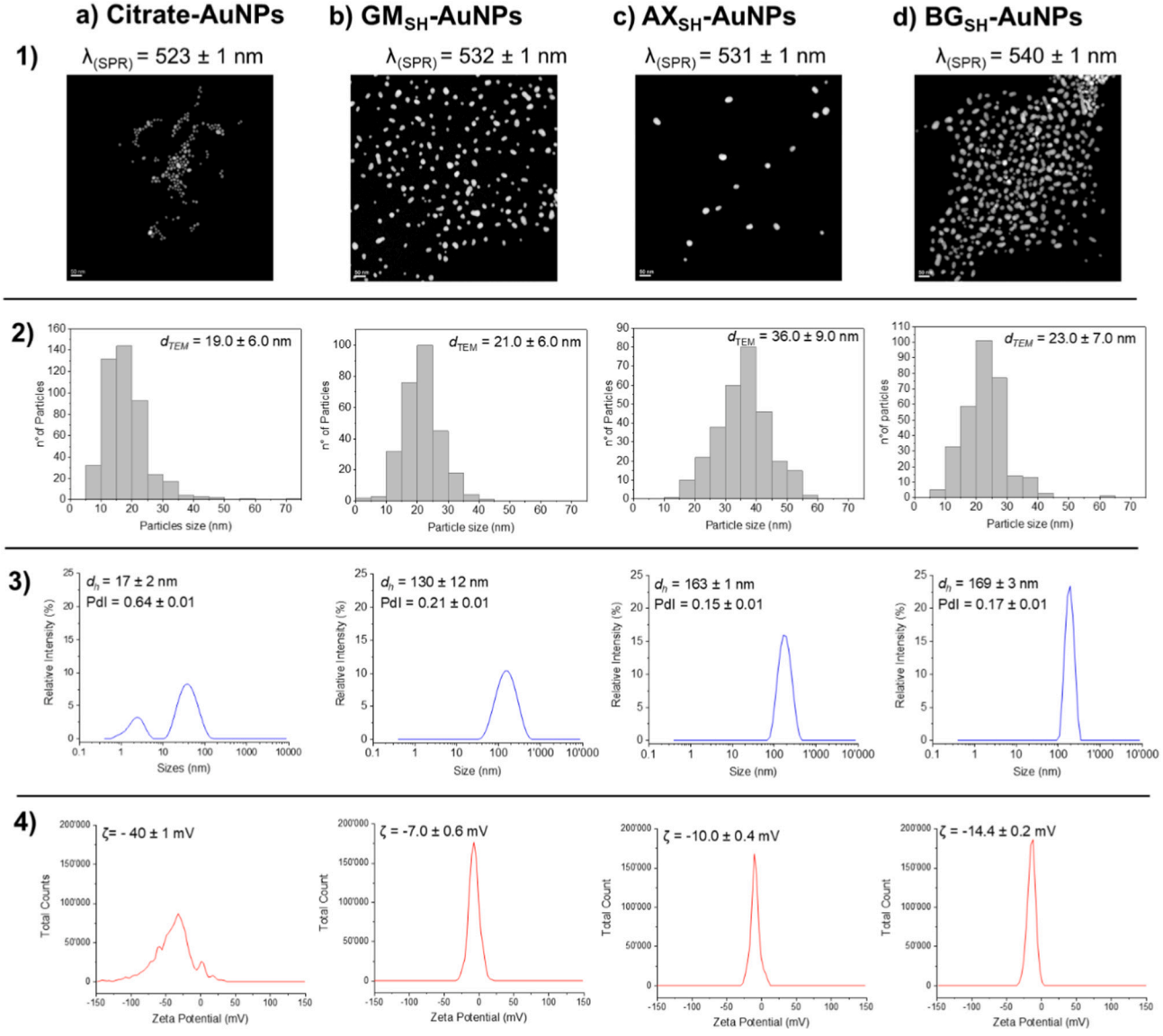

Fig. 2. 1) Surface Plasmon Resonance absorption band ($\lambda_{(SPR)}$), and TEM images of: a) Citrate-AuNPs, b) GM_{SH}-AuNPs, c) AX_{SH}-AuNPs, and d) BG_{SH}-AuNPs. 2) Size distribution, 3) Intensity-based DLS measurements, and 4) Zeta Potential (ζ) analysis of the same samples.

($\lambda_{(SPR)}$) of citrate-AuNPs before and after functionalization on the gold surface with the different thiolated fibers was measured by UV–vis spectrometry. Before the self-assembly mechanism with the thiolated polysaccharides, citrate-AuNPs shown a strong absorption at $\lambda_{(SPR)} = 523 \pm 1$ nm. As reported in the literature, a relatively small red-shift of the maximum $\lambda_{(SPR)}$ is evidence of successful functionalization (Lala et al., 2002). Indeed, the absorption band moved its center point from 523 ± 1 nm to 532 ± 1 nm, 531 ± 1 nm, and 542 ± 1 nm after displacement of citrate with GM_{SH}, AX_{SH}, and $BG_{SH,}$ respectively (for UV–Vis spectra, see Fig. S2). The morphology and size analysis of citrate-AuNps and glyco-AuNPs was performed by TEM (Fig. 2.1). All the synthesized particle samples presented a spherical appearance but with different spatial arrangement of the particles in solution, emphasizing the influence of the molecular weight, type, and surface density of the linked polysaccharide on the architecture of the colloidal suspension, as explained in the previous publication (Lupo et al., 2021).

The particle size distribution of each glyco-AuNPs (d_{TEM}) before and after the coupling reaction was derived from the area of the Au-cores. While functionalization of the citrate-AuNP did not significantly change the size distribution of the particles for the two shorter polysaccharides galactomannan and β-glucan (range of 19–23 nm), a clear increase was observed for the particles functionalized with arabinoxylan (d_{TEM} [AX_{SH}-AuNps = 36.0 nm]; Fig. 2.2 Potentially, in the latter case, the ligand exchange mechanism is favored on gold particles with a larger surface area, allowing the polymer chains to be more widely spaced on the particle surface, minimizing the steric hindrance effect. In addition, fewer polymer chains of $AX_{SH}$are tailored to small AuNPs, which are therefore poorly stabilized due to the lower coverage, leading to partial sintering of AuNPs to a size that is stable, with sufficient chain coverage for this size.

In addition, glyco-AuNPs were characterized by dynamic light scattering and zeta potential for determining their hydrodynamic radius (d_h) and the surface charge (ζ), respectively. As expected, upon functionalization with the thiolated ligand, the average diameter of the particles as well as the zeta potential increased significantly (Fig. 2.3 and .4) in agreement with our previous publication (Lupo et al., 2021).

3.3.1. Ligand surface density of glyco-gold nanoparticles

The amount of labelled polysaccharide bound to the AuNPs core was determined by anthrone/H_2SO_4 assay (Table 2). All the parameters shown in Table 2 were calculated by considering the number average molecular weight (M_n) of the oxidized fibers, as this number refers to the size of a single polymer chain, whereas M_n of the thiolated fibers came from the assembly of at least two polymer chains, assuming the dimerization mechanism of the thiol group to disulfide. As expected, the coupling efficiency decreased with increasing M_n of the polysaccharide, namely 36%, 21%, and 20% for thiolated GM, BG, and AX, respectively. The ligand-exchange reaction was disadvantaged for the longer polysaccharide due to higher steric hindrance and a lower diffusion rate. However, it is important to mention that the nmol of fiber chains/ng AuNPs added for AX_{SH}-AuNPs were 3-fold lower than nmol of fiber chains added for GM_{SH} and BG_{SH}-AuNPs, justifying the lower value of coupling efficiency obtain for the arabinoxylan-tethered particles.

As already specified in our previous publication, the M_n and $Đ$ of the linked polysaccharide might influence the spatial arrangement of the particles in solution (Lupo et al., 2021). However, with this study, all the samples had a comparable moderate dispersity, and hence only the effect of chain length could be assessed here. Smaller chains (*e.g.* GM_{SH}) react more efficiently than longer chains (AX_{SH}) due to the faster diffusion and leading a higher polysaccharide chain-density on the particles surface (37, 2, and 14 chains/AuNP for GM_{SH}-AuNP, AX_{SH}-AuNP, and BG_{SH}-AuNP, respectively.

3.4. Interaction study with small molecules

3.4.1. Interaction study with ITC

The molecular interactions between hydrolyzed galactomannan, hydrolyzed arabinoxylan, and standard β-glucan with different small molecules, namely gallic acid (GA), *trans*-cinnamic acid (*t*-CA), acetylsalicylic acid (ASA), and acetaminophen (ACM) were evaluated by ITC. No interaction was detected between any of the polysaccharides and acetaminophen, while for all the other ligands a spontaneous interaction was observed, since a Gibbs' energy ($\Delta G = \Delta H - T\Delta S$) that was negative ($\Delta G < 0$) was measured (Table 3). All the conducted experiments presented a negative value of the binding enthalpy (ΔH), which reflects the strength of the interaction between the molecular partners, and generally relates to van der Waals, hydrogen bonds, and ion pair interactions at the binding interface. The negative ΔH values suggest the formation of energetically favorable exothermic non-covalent interactions between galactomannan, arabinoxylan, β-glucan and the small molecules (Du et al., 2016). Specifically, for all the samples, entropically-driven associations were observed ($|\Delta H| < |T\Delta S|$). These types of associations are generally related to a combination of hydrophobic/H-bonding interactions, loss of water molecules, and conformational changes of the polysaccharide (Bronowska, 2011). For all the cases shown in Table 3, the change in enthalpy upon formation of the complex was relatively low (-0.8 kcal/mol $< \Delta H < -3.5$ kcal/mol), suggesting that the binding event was also driven by an additional thermodynamic phenomenon called enthalpy-entropy compensation. Entropy (ΔS) is a measure of the disorder of molecules in a system, and its positive and negative values denotes the overall increase and decrease in degrees of the freedom of the system, respectively. The total entropy change associated with binding (ΔS) is a combination of different energetic factors, namely the solvent release entropy change, which has favorable contribution, the conformational entropy change, that can be favorable or unfavorable depending on the degree of freedom of the complex, and the loss of translational and rotational degrees of freedom of the biomolecule and ligand upon complex formation, which gives an unfavorable contribution. These individual components influence the magnitude of the net entropy change, with positive or negative entropy change contribution, favoring or disfavoring the binding free energy, respectively (O'Brien et al., 2017). Therefore, the binding reaction (ΔG) should address entropic unfavorable contribution through a large gain in solvent release entropy that would be compensated by loss of enthalpy, or favorable biomolecule-ligand interactions that lead to a negative ΔH (Amzel, 2000). What can be hypothesized for our interaction study is that through the formation of the polysaccharide-small molecule complex, a conformational change happens in the fiber, which limits the degree of freedom of the complex and therefore has a detrimental impact on the entropic binding

Table 2
M_n and $Đ$ values of the oxidized materials (GM_{OX}, AX_{OX}, and BG_{OX})after treatment with $NaIO_4$. Amounts in nmol of thiolated polysaccharides (PS_{SH}) per ng of AuNPs added and per ng of AuNPs conjugated. Coupling efficiency (%) of thiolated polysaccharides expressed as the ratio between $PS_{SH(conjugated)}$ and $PS_{SH(added)}$. Number of repeating units [RU] per AuNPs. Number of conjugated polymer chains ($PS_{SH(conjugated)}$) per AuNP.

Samples	M_n (kDa)	$Đ$ (M_w/Mn)	$PS_{SH(added)}$ (nmol/ng AuNP)	$PS_{SH(conjug.)}$ (nmol/ng AuNP)	Coupling efficiency	$\frac{n°RU}{n°AuNP}$	$\frac{n°PSSH(conjugated)}{n°AuNP}$
GM_{SH}-AuNP	19 ± 1	1.5 ± 0.01	63	22.5	36%	4393	37
AX_{SH}-AuNP	60 ± 2	1.5 ± 0.06	20	4	20%	773	2
BG_{SH}-AuNP	24 ± 1	1.4 ± 0.02	50	10.3	21%	2001	14

Table 3
Thermodynamic parameters of the interaction between gallic acid (GA), trans-cinnamic acid (*t*-CA), and acetylsalicylic acid (ASA) with hydrolyzed galactomannan (GM_{HCl}), hydrolyzed arabinoxylan (AX_{HCl}), and standard β-Glucan (BG), determined by ITC. Values of the constant of dissociation (K_d in μM), binding stoichiometry (*N*), binding energy (ΔG in kcal/mol), binding enthalpy (Δ*H* in kcal/mol), and binding entropy (−TΔ*S* in kcal/mol) are reported. All the analysis were performed in water.

Ligand	[Ligand] (μM)	K_d (μM)	*N*	Δ*G* (kcal/mol)	Δ*H* (kcal/mol)	−TΔ*S* (kcal/mol)
Sample Cell: 125 μM GM_{HCl}						
GA	1250	2.24 ± 0.75	0.70 ± 0.02	−7.71	−1.78 ± 0.08	−5.93
T-CA	1750	3.71 ± 0.68	1.45 ± 0.02	−7.41	−0.949 ± 0.02	−6.46
AsA	625	2.12 ± 0.36	0.36 ± 0.01	−7.74	−2.56 ± 0.07	−5.18
Sample Cell: 62.5 μM AX_{HCl}						
GA	800	3.99 ± 0.90	1.51 ± 0.03	−7.37	−1.67 ± 0.06	−5.70
t-CA	1250	5.53 ± 1.27	2.28 ± 0.06	−7.17	−0.910 ± 0.03	−6.26
AsA	1250	3.94 ± 0.67	1.38 ± 0.03	−7.38	−3.52 ± 0.10	−3.86
Sample Cell: 125 μM BG						
GA	625	2.02 ± 0.57	0.53 ± 0.01	−7.77	−1.24 ± 0.04	−6.54
t-CA	1250	3.05 ± 0.75	1.02 ± 0.02	−7.53	−0.844 ± 0.03	−6.68
AsA	625	2.44 ± 0.59	0.34 ± 0.01	−7.66	−2.97 ± 0.132	−4.69

contribution, which was compensated for by an increase in the enthalpy component.

An estimation of the affinity of the interaction between the ligand and the biomolecule was determined by measuring the dissociation constant (K_d). Generally, the smaller the dissociation constant, the more tightly bound the ligand is. Specifically, dissociation constant larger than 10^{-4} M indicates a weak biomolecule-ligand interaction (Liu et al., 2020). In our study all the formed complexes were on the order of 10^{-6} M (Table 3), and therefore, moderate binding interactions were formed upon addition of the small molecules into the sample cell. A common trend was observed for K_d values related to the interaction of the fibers with GA, *t*-CA and ASA. For all the tested polysaccharides, *t*-CA was the ligand with the highest binding constant ($K_d = 3.7 \pm 0.7$ μM for GM_{HCl}, $K_d = 5.5 \pm 1.3$ μM for AX_{HCl}, and $K_d = 3.1 \pm 0.8$ μM for BG), followed by GA and ASA. This suggested that *t*-CA had less affinity for galactomannan, arabinoxylan and β-Glucan than GA and ASA.

Comparing the chemical structures of GA and *t*-CA, with GA having three phenolic hydroxyl groups *vs.* none for *t*-CA, one can conclude that the additional peripheral hydroxyl groups may be responsible for a stronger and more extensive binding due the formation of intermolecular hydrogen bonds between the hydroxyl groups of GA and the oxygen atoms of the polysaccharide structure, resulting in an increase in the favorable binding enthalpy from $\Delta H_{(t\text{-}CA)} = -0.95$ kcal/mol to $\Delta H_{(GA)} = -1.78$ kcal/mol for GM_{HCl}, from $\Delta H_{(t\text{-}CA)} = -0.91$ kcal/mol to $\Delta H_{(GA)} = -1.67$ kcal/mol for AX_{HCl}, and from $\Delta H_{(t\text{-}CA)} = -0.844$ kcal/mol to $\Delta H_{(GA)} = -1.24$ kcal/mol for BG (Le Bourvellec et al., 2005; Phan et al., 2015).

For all the polysaccharide-ASA interactions, more negative values of enthalpy were measured compared to the enthalpy values obtained from the interaction between the same polysaccharides with GA and *t*-CA, indicating that for formation of polysaccharide-ASA molecular complexes, the H-binding interactions are more favorable than for interaction with the other two molecules (Dragan et al., 2017). The greater negative contribution of the enthalpy component in determining the binding energy of polysaccharide-ASA interaction might be also related to the lower pk_a value of the carboxylic acid group present in the acetylsalicylic acid molecule (pk_a (ASA) = 2.97) compared with that of carboxylic acid in gallic and cinnamic acid molecules ($pk_a = 4.5$ for both).

It is appropriate at this point to discuss why titration of the fiber with acetaminophen (ACM) does not produce any binding signal. The main difference between the ACM molecule and the other ligands used is the lack of a carboxylic acid group in its chemical structure, which could be crucial for interaction with the polymer chains. To verify the importance of the carboxylic acid group in determining whether the interaction occurs or not, experimental tests of interaction between β-glucan and propyl gallate, methyl vanillate and methyl syringate were conducted and the results obtained were compared with the corresponding non-esterified molecules *i.e.* with gallic acid, vanillic acid and syringic acid (data not shown) (Fig. 3). Indeed, measurements with the ITC showed no interaction between the BG polysaccharide and esterified derivatives confirming the hypothesis that the carboxylic acid group is essential for the interaction.

The binding stoichiometry (*N*), defined as the number of ligand binding sites on the polysaccharide molecule, was evaluated (Table 3). For all the fibers the interaction with *trans*-cinnamic acid (*t*-CA) presented the highest binding stoichiometry, with $N = 1.45 \pm 0.02$, 2.28 ± 0.06, and 1.02 ± 0.01, suggesting that the binding sites of the different fiber molecules saturated with *t*-CA at a molar ratio of about 2 for the *t*-CA/AX_{HCl} complex, 1 for *t*-CA/BG, and something in between for the *t*-CA/GM_{HCl} complex.

Within the fiber samples, AX_{HCl} was the fiber with the highest values of *N* for all the tested ligands, with $N = 1.51 \pm 0.03$, 2.28 ± 0.06, and 1.38 ± 0.03 for GA, *t*-CA, and ASA, respectively, while GM_{HCl} and BG had comparable values of *N*. Apart from the M_n and the size of the polysaccharide chain the conformation of the fiber in solution, the type of monosaccharides (hexose or pentose) and the chemical structure of the sugar units constituting the polysaccharide chain are factors that may potentially influence the number of sites available for interaction with the ligand molecule. The Mark-Houwink-Sakurada relationship, which describes the correlation between the intrinsic viscosity and molecular weight of a polymer in solution, is a useful tool for determining its conformation in solution, based on the values assumed by the parameter α. For $\alpha = 1.8$ a rigid rod conformation is expected, when $0.5 < \alpha < 0.8$, a semi-flexible or random coil conformation is usually assumed, and if the polymer adopts a compact conformation, α acquires values close to 0 (Halabalová et al., 2004). Based on the results obtained from the OMNISEC software, it was found that GM_{HCl}, AX_{HCl}, and BG possessed an α value that fell in the region of semi-flexible or random coil conformation, with $\alpha = 0.62 \pm 0.01$, $\alpha = 0.78 \pm 0.01$, $\alpha = 0.85 \pm 0.02$, for AX_{HCl}, GM_{HCl}, and BG, respectively. However, with GMH_{Cl} and BG leaning towards a more rigid, and less compact conformation than AX_{HCl}. Therefore, the greater flexibility of the arabinose polymer chains in solution can make arabinoxylan more prone to accept a binding molecule than galactomannan and β-glucan. In addition, the BG and GM chemical structure is characterized by a hexose type of monosaccharide, whereas AX is formed by pentoside constituents. This diversity could also explain the similar N values between BG and GM, which differ considerably from those assumed by AX, in addition to the most obvious cause, namely M_n, with BG and GMH_{Cl} being closest together, with a large gap to AX_{HCl}. More information related to the ITC interaction studies, namely the raw and fitted data, are reported in the supplementary information (Fig. S3).

Although the technical/experimental constraints used in this study require a reduced molecular weight sample for interaction studies, and since we are looking for direct molecular interaction effects, and not for

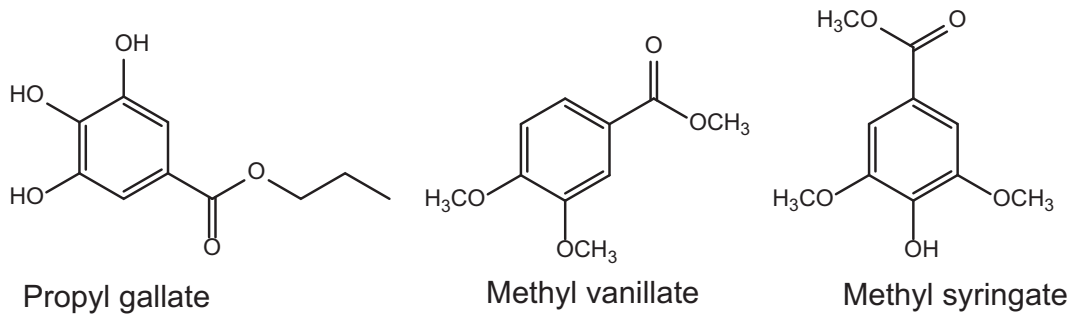

Fig. 3. Chemical structure of propyl gallate, methyl vanillate, and methyl syringate.

viscosity-related retention or gel-related entrapment, it can be assumed that any of the interaction result found for the shorter polysaccharide should also be conserved for the larger native samples, since the chemical composition and structure of the processed polysaccharides is largely conserved. Based on these observations, we can conclude that galactomannan (M_w = 69 kDa), arabinoxylan (M_w = 106 kDa), and β-glucan (M_w = 65 kDa) present in a food system, might partially prevent (or slow down) the intestinal absorption of small molecules, such as

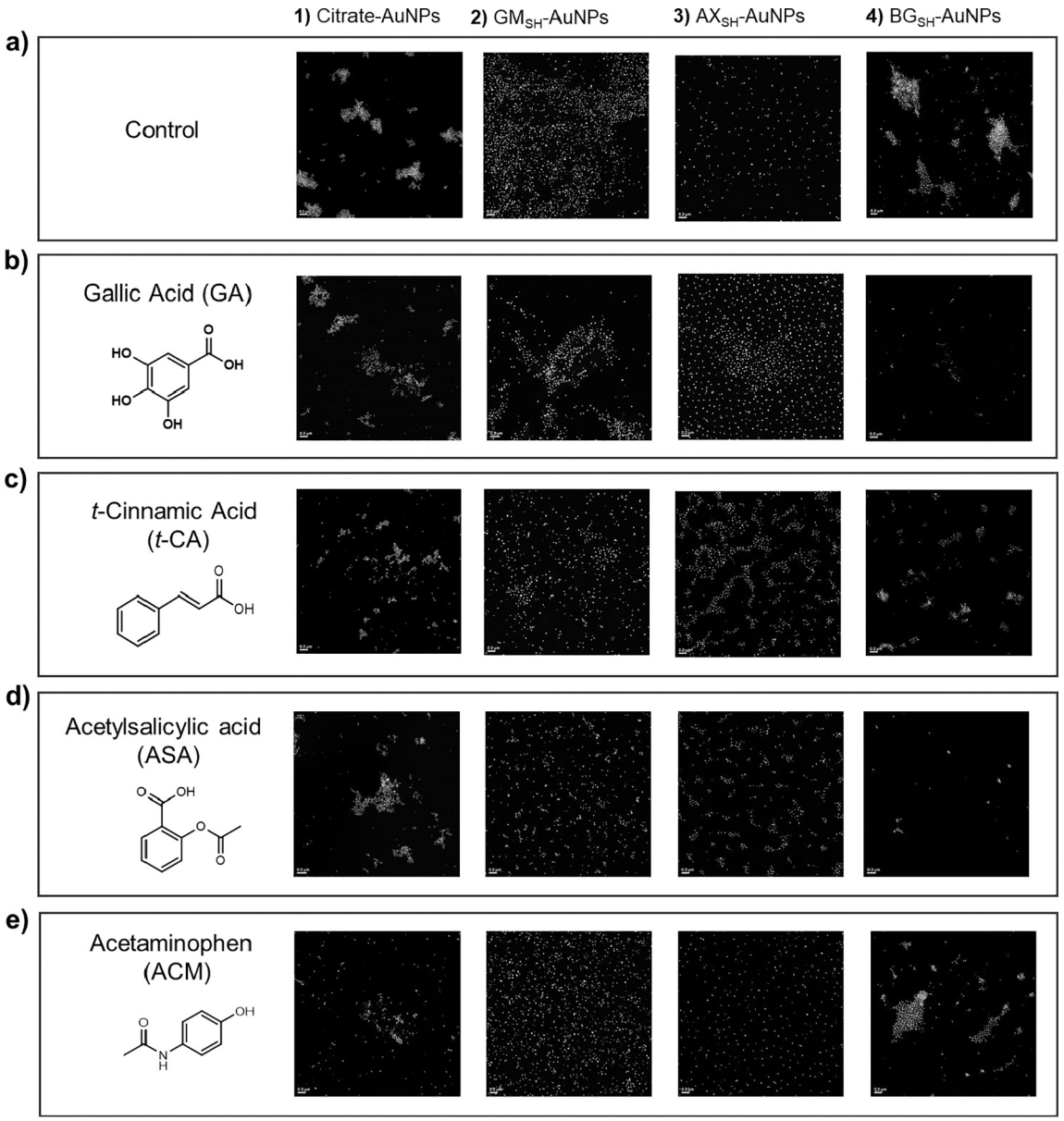

Fig. 4. TEM images of citrate, GM_{SH}, AX_{SH}, and BG_{SH} glyconanoparticles. The absolute concentration of each ligand in the particle samples was 50 μM. The overall concentration of the nanoparticles in the samples remained constant (7.8 nM Au particles). Scale bar are 0.2 μm for all the images.

gallic acid, cinnamic acid, and acetylsalicylic acid and similar compounds, by interacting with them and possibly affecting their bioavailability. This could be – depending on the extent of diminished bioavailability – especially consequential for drugs such as acetylsalicylic acid, commonly known as Aspirin.

3.4.2. Interaction study with TEM

A visual inspection of the interaction between the polysaccharide-coated gold nanoparticles and the ligands (GA, *t*-CA, ASA, ACM) was performed by TEM (Fig. 4). To reveal potential interaction, the spatial arrangement of the particles in solution was monitored upon addition of the ligand molecules. The introduction of each ligand to the citrate-AuNP material did not appear to significantly modify the arrangement of the particles in solution, suggesting that these molecules did not interact with the gold core (in Fig. 4, compare control 1.a to 1.b, 1.c, 1.d, and 1.e). Conversely, when the carboxylic acids GA, *t*-CA, and ASA were added to the particle solutions, a strong rearrangement of the colloidal particles was visible. For GM_{SH}-AuNps and AX_{SH}-AuNPs samples, it appeared that all three ligands could act as a bridge between the decorated gold nuclei to bring them closer together, leading to highly ordered clustering of particles in solution. However, the addition of acetaminophen (ACM) did not alter the spatial arrangement of all the fiber-coated nanoparticles (Fig. 4 box e) in comparison to citrate-AuNPs starting material, where water was added (Fig. 4 box a). This result confirmed the outcomes found by ITC experiments, where no binding isotherms were measured when the polysaccharides were titrated with ACM.

As we established in our previous publication, supramolecular interactions visible by TEM are favored for a lower surface density but higher molecular weight of the ligand anchored to the particle surface. The sample that best meet these requirements was AX_{SH}-AuNPs, with a $M_n(AX_{OX}) = 60$ kDa, and 2 polymer chains per Au core, compared to M_n (GM_{OX}) = 19 kDa, and 37 polymer chains per Au core, and $M_n(BG_{OX}) = 24$ kDa, with 14 polymer chains per Au core. Hence, this explains why the spatial realignment of the particles after the addition of the ligand molecule was the most pronounced for AX_{SH}-AuNPs, and therefore molecular interactions were more easily to be captured by screening of the sample with TEM, as visible in Fig. 4. When GA was added to the AX_{SH}-AuNPs, an increase in the density of particles was observed, which were highly evenly distributed (Fig. 4; 3.b), while the addition of *t*-CA and ASA resulted in the formation of highly organized nanoclusters (Fig. 4; 3.c, 3.d). These observations suggest that the AX polymer chains bound on the surface of the gold particles interact with GA, *t*-CA, and ASA, leading to a spatial re-distribution of the particles in solution. A slightly different situation was observed for GM_{SH}-AuNps, where bigger agglomeration of particles was formed after addition of GA (Fig. 4; 2.b). However, the addition of *t*-CA and ASA to the GM nanoparticles resulted in a similar behavior to that obtained with AX_{SH}.

The scenario was different for the BG glyconanoparticles, when comparing to the interactions exerted by AX. Upon incubation with GA and ASA, TEM imagines of BG glyconanoparticles showed an overall reduction of the gold density with formation of relatively small and diffuse aggregates, compared to the control. As determined by ITC, for β-glucan samples, the saturation of the polymer chain was reached at a very low ligand to biomacromolecule ratio (see Table 3 and Fig. S3c). In general, the lower the binding stoichiometry, the faster the substrate is saturated with the ligand during ITC, indicating only a few interaction sites on the polysaccharide structure, and therefore the formation of aggregates induced by the addition of a ligand which acts as a bridge between gold cores is unfavored as the ligand needs several anchor points for this bridge/aggregation to be formed. A slightly different situation was observed upon addition of *t*-CA to BG_{SH}-AuNPs (Fig. 4c.4), where indeed, larger clusters containing more particles were observed, in agreement with the higher binding stoichiometry (*N*) calculated by ITC. A validation experiment was carried out by exposing BG_{SH}-AuNPs to Calcofluor white under the same experimental conditions as for the other ligands. The specific binding of Calcofluor white to β-glucan is very well-established (Nicholas et al., 1994), and could be also visualized by TEM as large nanoparticle clusters after 3 h of incubation (Fig. S4), validating the reliability of this method in observing molecular interactions between two species.

4. Conclusion

In this study, two different analytical methods were used to evaluate supramolecular interactions between soluble dietary fibers (galactomannan, arabinoxylan and cereal β-glucan) and four small molecules. In a first stage, ITC was successfully employed to determine the dissociation constant (K_d), binding stoichiometry (*N*), enthalpy (ΔH), and entropy (ΔS) of the interaction. From the analysis of the data set obtained with ITC, acetaminophen (ACM) was the only small molecule of the set of four with no detectable interaction with the different fibers. For all other tested ligands (gallic acid (GA), *trans*-cinnamic acid (*t*-CA), and acetylsalisylic acid (ASA)), moderate affinity ($K_d \sim 10^{-6}$ M), and spontaneous interactions ($\Delta G < 0$) were observed. The interactions were mainly driven by an entropic factor, presumably with hydrophobic type associations, and possible conformational changes of the polysaccharide. However, the enthalpy contribution (hydrogen interaction) is also significant, especially regarding interactions with the ASA molecule.

The nature of the ligand greatly influenced the quality of the interaction; in particular, in pure aqueous solutions of fiber and small molecule, the carboxylic group of acetylsalicylic acid ($pk_a = 2.97$), gallic acid and *trans*-cinnamic acid ($pk_a = 4.5$) was absolutely crucial for the formation of the complex. In addition a stronger interaction (lower K_d) was promoted when the ligand carried hydroxyl groups, which fostered hydrogen bonds formation with the polysaccharides. Finally, the conformation of the dietary fiber in solution might alter the success of the interaction. From our results appeared that more flexible molecules promote the contact with the ligand, while more rigid polysaccharides disfavor the interaction. However, also other factors such as the chain length may also participate in guiding the interaction.

In the second approach, TEM was used for a visual inspection of the samples to check the possible fiber-ligand interaction based on the spatial rearrangement of the glyco-gold nanoparticles after addition of the binding molecule. Specifically, supramolecular interactions visible as highly organized particle clusters were favored for galactomannan and arabinoxylan, when exposed to gallic acid, acetylsalicylic acid, and *trans*-cinnamic acid, while acetaminophen, which showed no interaction with ITC, also did not interfere with the order of the particles in solution.

From the results obtained from the combination of ITC and TEM analysis, we can conclude that direct interactions at the molecular level, which go beyond viscosity and/or gel entrapment mechanisms, exist at least between galactomannan, arabinoxylan, β-glucan, and gallic acid, acetylsalicylic acid, and *trans*-cinnamic acid. Furthermore, since the chemical structure of these polysaccharides was largely conserved even in the smallest M_w, the results achieved with these smaller fibers should also apply to some extent in the native SDF. In conclusion, this study can be considered a valuable analytical tool to estimate the key parameters involved in the interaction between neutral dietary fibers and small molecules, leading to a better understanding of the mechanism underlying their complexation and consequently to an optimization of their use in food industry applications.

CRediT authorship contribution statement

Cristina Lupo: Conceptualization, Methodology, Formal analysis, Investigation, Writing - original draft, Writing – review & editing, Visualization. Samy Boulos: Conceptualization, Methodology, Writing – review & editing, Supervision, Funding acquisition. Fabian Gramm Formal analysis, Investigation, Writing - review & editing, Visualization. Xiaowen Wu: Formal analysis, Investigation, Writing - review & editing.

Laura Nyström: Resources, Conceptualization, Writing - review & editing, Supervision, Project administration, Funding acquisition.

Declaration of competing interest

The authors declare that they have no known competing financial interests or personal relationships that could have appeared to influence the work reported in this paper.

Acknowledgements

The authors are very thankful to Victorelli Francesca for the DLS support and data exportation assistance.

Funding

This work was supported by European Research Council ERC, under the European Union's Horizon 2020 research and innovation programme (Grant agreement No. 679037).

Appendix A. Supplementary data

Supplementary data to this article can be found online at https://doi.org/10.1016/j.carbpol.2022.119229.

References

Amzel, L. M. (2000). Calculation of entropy changes in biological processes: Folding, binding, and oligomerization. *Methods in Enzymology, 323*, 167–177.
Anderson, J. W., Baird, P., Davis, R. H., Ferreri, S., Knudtson, M., Koraym, A., & Williams, C. L. (2009). Health benefits of dietary fiber. *Nutrition Reviews, 67*(4), 188–205.
Bagiyan, G., Koroleva, I., Soroka, N., & Ufimtsev, A. (2003). Oxidation of thiol compounds by molecular oxygen in aqueous solutions. *Russian Chemical Bulletin, 52*(5), 1135–1141.
Balasubramanian, S. K., Yang, L., Yung, L.-Y. L., Ong, C.-N., Ong, W.-Y., & Liya, E. Y. (2010). Characterization, purification, and stability of gold nanoparticles. *Biomaterials, 31*(34), 9023–9030.
Börjesson, M., Larsson, A., Westman, G., & Ström, A. (2018). Periodate oxidation of xylan-based hemicelluloses and its effect on their thermal properties. *Carbohydrate Polymers, 202*, 280–287.
Bronowska, A. K. (2011). Thermodynamics of ligand-protein interactions: Implications for molecular design. In *Thermodynamics-interaction studies-solids, liquids and gases*. IntechOpen.
Colleoni-Sirghie, M., Fulton, D. B., & White, P. J. (2003). Structural features of water soluble (1, 3)(1, 4)-β-D-glucans from high-β-glucan and traditional oat lines. *Carbohydrate Polymers, 54*(2), 237–249.
Dragan, A. I., Read, C. M., & Crane-Robinson, C. (2017). Enthalpy–entropy compensation: The role of solvation. *European Biophysics Journal, 46*(4), 301–308.
Du, X., Li, Y., Xia, Y.-L., Ai, S.-M., Liang, J., Sang, P., & Liu, S.-Q. (2016). Insights into protein–ligand interactions: Mechanisms, models, and methods. *International Journal of Molecular Sciences, 17*(2), 144.
Eder, S., Zueblin, P., Diener, M., Peydayesh, M., Boulos, S., Mezzenga, R., & Nyström, L. (2021). Effect of polysaccharide conformation on ultrafiltration separation performance. *Carbohydrate Polymers, 260*, Article 117830.
Edwards, C., Blackburn, N., Craigen, L., Davison, P., Tomlin, J., Sugden, K., & Read, N. (1987). Viscosity of food gums determined in vitro related to their hypoglycemic actions. *The American Journal of Clinical Nutrition, 46*(1), 72–77.
Fernandes, A., Brás, N., & r. F., Mateus, N., & de Freitas, V.. (2014). Understanding the molecular mechanism of anthocyanin binding to pectin. *Langmuir, 30*(28), 8516–8527.
Gallaher, D. D., & Schaubert, D. R. (1990). The effect of dietary fiber type on glycated hemoglobin and renal hypertrophy in the adult diabetic rat. *Nutrition Research, 10*(11), 1311–1323.
Gunness, P., & Gidley, M. J. (2010). Mechanisms underlying the cholesterol-lowering properties of soluble dietary fibre polysaccharides. *Food & Function, 1*(2), 149–155.
Halabalová, V., Šimek, L., Dostál, J., & Bohdanecký, M. (2004). Note on the relation between the parameters of the Mark-Houwink-Kuhn-Sakurada equation. *International Journal of Polymer Analysis and Characterization, 9*(1–3), 65–75.
Kahkeshani, N., Farzaei, F., Fotouhi, M., Alavi, S. S., Bahramsoltani, R., Naseri, R., & Farzaei, M. H. (2019). Pharmacological effects of gallic acid in health and diseases: A mechanistic review. *Iranian Journal of Basic Medical Sciences, 22*(3), 225.
Lala, N., Chittiboyina, A., Chavan, S., & Sastry, M. (2002). Biotinylation of colloidal gold particles using interdigitated bilayers: A UV–visible spectroscopy and TEM study of the biotin–avidin molecular recognition process. *Colloids and Surfaces A: Physicochemical and Engineering Aspects, 205*(1–2), 15–20.
Le Bourvellec, C., Bouchet, B., & Renard, C. (2005). Non-covalent interaction between procyanidins and apple cell wall material. Part III: Study on model polysaccharides. *Biochimica et Biophysica Acta (BBA)-General Subjects, 1725*(1), 10–18.
Liu, X., Le Bourvellec, C., & Renard, C. M. (2020). Interactions between cell wall polysaccharides and polyphenols: Effect of molecular internal structure. *Comprehensive Reviews in Food Science and Food Safety, 19*(6), 3574–3617.
Lupo, C., Boulos, S., & Nyström, L. (2020). Influence of partial acid hydrolysis on size, dispersity, monosaccharide composition, and conformation of linearly-branched water-soluble polysaccharides. *Molecules, 25*(13), 2982.
Lupo, C., Boulos, S., Delle Vedove, C., Gramm, F., & Nyström, L. (2021). Dietary fiber-tethered gold nanoparticles: An innovative analytical tool for probing interactions. *Polysaccharides, 2*(2), 497–518.
Marasca, E., Boulos, S., & Nyström, L. (2020). Bile acid-retention by native and modified oat and barley β-glucan. *Carbohydrate Polymers, 236*, Article 116034.
Nicholas, R., Williams, D. W., & Hunter, P. (1994). Investigation of the value of β-glucan-specific fluorochromes for predicting the β-glucan content of the cell walls of zoopathogenic fungi. *Mycological Research, 98*(6), 694–698.
Nishinari, K., Takemasa, M., Fang, Y., Hossain, K. S., Tsumura, Y., Sone, Y., & Emoto, M. (2020). Effects of xyloglucan with different molar masses on glucose in blood. *Food Hydrocolloids, 108*, Article 105727.
O'Brien, R., Markova, N., & Holdgate, G. A. (2017). Thermodynamics in drug discovery. *Applied Biophysics for Drug Discovery*, 7–28.
Pavli, M., Baumgartner, S., Kos, P., & Kogej, K. (2011). Doxazosin–carrageenan interactions: A novel approach for studying drug–polymer interactions and relation to controlled drug release. *International Journal of Pharmaceutics, 421*(1), 110–119.
Phan, A. D. T., Netzel, G., Wang, D., Flanagan, B. M., D'Arcy, B. R., & Gidley, M. J. (2015). Binding of dietary polyphenols to cellulose: Structural and nutritional aspects. *Food Chemistry, 171*, 388–396.
Pitkanen, L., Virkki, L., Tenkanen, M., & Tuomainen, P. (2009). Comprehensive multidetector HPSEC study on solution properties of cereal arabinoxylans in aqueous and DMSO solutions. *Biomacromolecules, 10*(7), 1962–1969.
Queenan, K. M., Stewart, M. L., Smith, K. N., Thomas, W., Fulcher, R. G., & Slavin, J. L. (2007). Concentrated oat β-glucan, a fermentable fiber, lowers serum cholesterol in hypercholesterolemic adults in a randomized controlled trial. *Nutrition Journal, 6*(1), 1–8.
Tamaki, Y., Teruya, T., & Tako, M. (2010). The chemical structure of galactomannan isolated from seeds of Delonix regia. *Bioscience, Biotechnology, and Biochemistry, 74*(5), 1110–1112.
Turula, V. E., Jr., Gore, T., Singh, S., & Arumugham, R. G. (2010). Automation of the anthrone assay for carbohydrate concentration determinations. *Analytical Chemistry, 82*(5), 1786–1792.
Vold, I. M., & Christensen, B. E. (2005). Periodate oxidation of chitosans with different chemical compositions. *Carbohydrate Research, 340*(4), 679–684.
Wang, X., Ramström, O., & Yan, M. (2009). A photochemically initiated chemistry for coupling underivatized carbohydrates to gold nanoparticles. *Journal of Materials Chemistry, 19*(47), 8944–8949.
Zacherl, C., Eisner, P., & Engel, K.-H. (2011). In vitro model to correlate viscosity and bile acid-binding capacity of digested water-soluble and insoluble dietary fibres. *Food Chemistry, 126*(2), 423–428.